Assessing the Accuracy of the Cloud and Water Vapor Fields in the Hurricane WRF (HWRF) Model Using Satellite Infrared Brightness Temperatures

JASON A. OTKIN, WILLIAM E. LEWIS, AND ALLEN J. LENZEN

Cooperative Institute for Meteorological Satellite Studies, University of Wisconsin–Madison, Madison, Wisconsin

BRIAN D. MCNOLDY AND SHARANYA J. MAJUMDAR

Rosenstiel School of Marine and Atmospheric Science, University of Miami, Miami, Florida

(Manuscript received 13 September 2016, in final form 7 March 2017)

ABSTRACT

In this study, cycled forecast experiments were performed to assess the ability of different cloud microphysics and cumulus parameterization schemes in the Hurricane Weather Research and Forecasting (HWRF) Model to accurately simulate the evolution of the cloud and moisture fields during the entire life cycle of Hurricane Edouard (2014). The forecast accuracy for each model configuration was evaluated through comparison of observed and simulated *Geostationary Operational Environmental Satellite-13* (*GOES-13*) infrared brightness temperatures and satellite-derived tropical cyclone intensity estimates computed using the advanced Dvorak technique (ADT). Overall, the analysis revealed a large moist bias in the mid- and upper troposphere during the entire forecast period that was at least partially due to a moist bias in the initialization datasets but was also affected by the microphysics and cumulus parameterization schemes. Large differences occurred in the azimuthal brightness temperature distributions, with two of the microphysics schemes producing hurricane eyes that were much larger and clearer than observed, especially for later forecast hours. Comparisons to the forecast 10-m wind speeds showed reasonable agreement (correlations between 0.58 and 0.74) between the surface-based intensities and the ADT intensity estimates inferred via cloud patterns in the upper troposphere. It was also found that model configurations that had the smallest differences between the ADT and surface-based intensities had the most accurate track and intensity forecasts. Last, the cloud microphysics schemes had the largest impact on the forecast accuracy.

1. Introduction

Given the high socioeconomic costs associated with hurricanes and the need for more accurate forecasts that can be used to lessen their detrimental impacts on vulnerable coastal communities, substantial effort has been directed in recent years toward reducing tropical cyclone (TC) forecast track and intensity errors. Overall, forecast track errors have steadily decreased during the past decade; however, similar reductions in intensity errors have been more elusive. Large intensity errors in numerical weather prediction models can occur due to limited predictability of eyewall replacement cycles (Houze et al. 2007; Zhu et al. 2015) and rapid intensification events (e.g., Elsberry et al. 2007; Kaplan et al. 2010; Lee et al. 2016), both of which can lead to large changes in TC intensity over short time periods. The persistence of large intensity errors over longer forecast lead times could also result from systemic errors in the spatial distribution of latent heating caused by inaccuracies in the simulated cloud field (e.g., Liu and Moncrieff 2007). For example, differences in how microphysics parameterization schemes partition cloud condensate in the upper troposphere between different cloud hydrometeor species, combined with large differences in total cloud mass, can strongly modulate the vertical distribution of latent heat release. Other components of the forecast model such as the planetary boundary layer and cumulus parameterization schemes also exert a strong influence on the simulated cloud field through impacts on subgrid-scale moisture, heat, and momentum fluxes. Modifications to the distribution of latent heat release can lead to large differences in the vertical circulation and upper-level outflow pattern, which in turn can have a significant impact on TC track and intensity forecasts (e.g., Wu and Wang, 2001; Wang 2009).

Corresponding author: Jason A. Otkin, jason.otkin@ssec.wisc.edu

DOI: 10.1175/MWR-D-16-0354.1

Many previous studies have examined the sensitivity of TC forecast errors to the assumptions made by different model parameterization schemes. Large differences have been found in TC intensity, structure, and rainfall when different microphysics, cumulus, and planetary boundary layer schemes are used. For microphysics schemes, conversion processes such as condensation, melting, and evaporation between different hydrometeor species and their feedback to the large-scale environment can significantly impact the TC intensity (e.g., Pattnaik and Krishnamurti 2007a,b, 2011; Fovell and Su, 2007; Fovell and Corbosiero 2009; Fovell et al. 2010). The timing of rapid intensification events and the intensity of simulated TCs after several days of model integration has also been shown by Smith and Thomsen (2010) to be sensitive to different components of the planetary boundary layer scheme such as the vertical eddy diffusivity and surface drag coefficient. Indeed, Bao et al. (2012) showed that uncertainties in the planetary boundary layer and microphysics parameterization schemes have comparably large impacts on the intensity and structure of simulated TCs. Subgrid scale detrainment processes and the vertical transport of momentum, heat, and moisture represented by cumulus parameterization schemes can also strongly influence cloud morphology and the distribution of latent heat release, with attendant changes in TC structure and intensity (e.g., Davis and Bosart, 2002; Mukhopadhyay et al. 2011; Deshpande et al. 2012; Nasrollahi et al. 2012).

Though many prior studies have used traditional TC verification metrics such as track and intensity errors to evaluate the model sensitivity to different parameterization schemes and assumptions, few have done so using satellite observations even though they provide valuable information about TC intensity and the spatial and temporal distribution of clouds and water vapor. Airborne and land-based Doppler radars also provide detailed information about the cloud field; however, their limited spatial coverage and incomplete sampling hinders their use as a routine model evaluation tool. The so-called model-to-satellite approach in which model simulated fields such as temperature, water vapor, and cloud mixing ratios, are converted into simulated satellite brightness temperatures using a forward radiative transfer model has gained widespread acceptance as a useful method to evaluate the accuracy of weather and climate model forecasts. This approach has been used to assess the ability of models to produce accurate cloud and moisture forecasts (e.g., Karlsson 1996; Rikus 1997; Chaboureau et al. 2000; Tselioudis and Jakob 2002; Lopez et al. 2003; Grasso and Greenwald, 2004; Sun and Rikus 2004; Otkin and Greenwald 2008; Otkin et al. 2009), identify parameter sensitivities in microphysics schemes (Chaboureau and Pinty 2006; Grasso et al. 2014), and generate realistic brightness temperature datasets used as a proxy for future satellite sensors (Otkin et al. 2007; Grasso et al. 2008; Feltz et al. 2009; Bikos et al. 2012).

Recent studies by Jankov et al. (2011), Van Weverberg et al. (2013), and Cintineo et al. (2014) have shown that the spatial and temporal distribution of ice clouds in the upper troposphere can vary greatly depending upon which microphysics parameterization scheme is employed, whereas Thompson et al. (2016) demonstrated the importance of properly coupling the cloud microphysics and radiation parameterization schemes when simulating ice cloud radiative properties. Y. Jin et al. (2014) showed that errors in TC track and intensity forecasts were smaller when using a more sophisticated cloud microphysics scheme that predicts two moments of the particle size distribution. A large cold bias in the simulated infrared brightness temperatures associated with an overabundance of ice clouds was also eliminated when using the more sophisticated scheme. Taken together, these studies demonstrate the sensitivity of the cloud field to the assumptions made by different parameterization schemes.

In this study, we assess the accuracy of the cloud and water vapor fields in Hurricane Weather Research and Forecasting (HWRF) Model forecasts obtained when using different cloud microphysics and cumulus parameterization schemes. Cycled 5-day forecasts covering the entire life cycle of Hurricane Edouard, which briefly became a major hurricane in the central Atlantic in 2014, were performed for each model configuration. The forecast accuracy will be assessed through comparisons of observed and simulated infrared brightness temperatures, satellite-derived TC intensity estimates, and standard verification of simulated track and intensity metrics against the National Hurricane Center (NHC) best track (BT) dataset. The paper is organized as follows. The HWRF Model simulations and satellite datasets are described in section 2. Results are shown in section 3 with conclusions presented in section 4.

2. Datasets and methodology

a. HWRF Model configurations

The model simulations evaluated during this study were performed using the 2015 version of the operational HWRF Model maintained and supported by the Developmental Testbed Center (Bernardet et al. 2015). The complete modeling and data assimilation system (revision 4463) was installed on the "jet" supercomputer located at the Earth System Research Laboratory in January 2016. HWRF is a primitive equation, nonhydrostatic coupled atmosphere–ocean model that uses the Nonhydrostatic Mesoscale Model dynamic core and the Princeton Ocean Model for Tropical Cyclones (Yablonsky et al. 2015) to

predict changes in sea surface temperatures. The simulations contained three two-way interactive nested domains with 18, 6, and 2-km horizontal grid spacing, respectively. The parent domain covers an area spanning approximately 80° × 80°, with the inner domains covering 12° × 12° and 7.1° × 7.1°, respectively. The initial center locations of the parent and inner domains vary for each forecast cycle and are dictated by the observed location of the TC center at the beginning of the forecast period. The parent domain remains fixed during the entire forecast period, whereas the inner two domains move with time so that they remain centered on the TC. The vortex following algorithm identifies the TC center based on a set of "fix locations" that depict minima in sea level pressure and geopotential height or maxima in wind speed and vorticity in the lower troposphere. The TC center is defined as the mean of these fix locations. The model top is set to 2 hPa with 61 levels on a terrain-following vertical coordinate system. Complete details can be found in Tallapragada et al. (2015).

Cycled forecast experiments were performed for eight model configurations that employed different cloud microphysics and cumulus parameterization schemes, but were otherwise identical. Four microphysics schemes were evaluated, including the Ferrier scheme that was operational in 2014, the Ferrier–Aligo scheme that became operational in 2015, and two other schemes that are being considered for inclusion in future versions of the operational HWRF Model. These schemes include the Thompson microphysics and a special version of the Ferrier–Aligo scheme that contains separate horizontal and vertical advection tendencies for each hydrometeor species. The version of the Ferrier scheme used by HWRF is based on the Eta Grid-Scale Cloud and Precipitation microphysics scheme that has been modified for use in tropical environments (Ferrier 2005). It predicts changes in mass mixing ratios for four hydrometeor species including cloud water, rain, cloud ice, and precipitation ice (e.g., snow, graupel, and sleet). The individual mixing ratios are combined into a total condensate variable prior to computing the advection terms to reduce computational expense and then diagnostically separated into multiple species afterward. The Ferrier–Aligo scheme is a modified version of the tropical Ferrier scheme that was developed to improve simulations of deep convection in high-resolution numerical weather prediction models (Aligo et al. 2014). Like the older Ferrier scheme, the operational version of the Ferrier–Aligo scheme combines all of the hydrometeor mixing ratios into one quantity before calling the advection procedure. Recent work however has removed this constraint so that the advection tendencies are computed separately for each cloud species. This version of the scheme is known as the advected Ferrier–Aligo scheme. Last, the Thompson scheme includes prognostic equations for cloud water, rain, ice, snow, and graupel mixing ratios (Thompson et al. 2008). Unlike the other schemes, it is a hybrid double moment scheme that also predicts the number concentrations for cloud ice and rain.

To assess the forecast sensitivity to the cumulus parameterization scheme, each of the microphysics schemes was paired to either the simplified Arakawa–Schubert (SAS) scheme or to a newer version of the scheme known as the scale-aware SAS (SASAS) scheme. The cumulus scheme was only used on the outer two domains; thus, convection was explicitly represented on the innermost domain. The SAS scheme is based on the scheme described by Arakawa and Schubert (1974) that was subsequently simplified for operational use by Grell (1993) to consider only one cloud top at a specified time and location rather than a full spectrum of cloud sizes as was done in the original scheme. The scheme was revised to make cumulus convection stronger and deeper by increasing the maximum allowable cloud base mass flux and by having convective overshooting from a single cloud top. In the SAS scheme, convection depends on the cloud-work function, which is a quantity that is derived from the temperature and water vapor profiles in each model column. When the cloud-work function exceeds a certain threshold, the parameterizations are triggered and the mass flux of the cloud is determined using a quasi-equilibrium assumption. The temperature and moisture profiles are adjusted toward the equilibrium cloud-work function within a specified time scale using the mass flux, which is also allowed to transport momentum vertically in the column (Tallapragada et al. 2015). Recent work by Arakawa and Wu (2013) has generalized the framework for cumulus parameterization so that it can be applied to any horizontal resolution. This version of the scheme, known as the scale-aware SAS, is necessary for grid sizes less than 10 km where updrafts become partially or fully resolved. It permits a smooth transition between parameterized and explicit simulation of cloud-scale processes as the resolution increases by allowing the fractional area covered by convective updrafts in each grid box to approach one at higher resolutions. Table 1 lists the cumulus and microphysics parameterization schemes employed by each model configuration, along with the simulation acronyms that will be used in the remainder of the paper.

Cycled forecast experiments were performed for each model configuration with the initial forecast starting at 0000 UTC on 12 September 2014 when Edouard was first declared a tropical storm. The storm steadily intensified in a generally favorable environment as it moved toward the northwest to become a hurricane on 14 September and then a major hurricane on 16 September with maximum sustained winds of 105 kt

TABLE 1. Simulation acronyms and cumulus and microphysics parameterization schemes used for each model configuration.

Simulation	Microphysics scheme	Cumulus scheme
FERR-SAS	Ferrier	Simplified Arakawa–Schubert (SAS)
FERR-SASAS	Ferrier	Scale-aware SAS (SASAS)
FA-SAS	Ferrier–Aligo	SAS
FA-SASAS	Ferrier–Aligo	SASAS
ADVFA-SAS	Advected Ferrier–Aligo	SAS
ADVFA-SASAS	Advected Ferrier–Aligo	SASAS
THOM-SAS	Thompson	SAS
THOM-SASAS	Thompson	SASAS

(1 kt = 0.5144 m s^{-1}) before rapidly weakening as it curved toward the northeast (Fig. 1). Edouard fell below hurricane strength on 19 September before becoming a remnant low shortly thereafter (Stewart 2014). The final forecast was initialized at 1200 UTC on 19 September.

Initial conditions for the model simulations were obtained from Global Forecast System (GFS) analyses. The cycled modeling runs were initiated every 6 h using the vortex relocation procedure described by Gopalakrishnan et al. (2012). The relocation procedure replaces the vortex from the GFS analysis with the vortex from the previous HWRF forecast after correcting it using the observed TC location and intensity. Conventional observations, including radiosondes, dropwindsondes, aircraft reports, surface observations, and scatterometer winds, were assimilated every 6 h on the inner two domains using the hybrid ensemble–variational Gridpoint Statistical Interpolation analysis system (Wang et al. 2013). Satellite-derived atmospheric motion vectors along with clear-sky infrared and microwave radiances from several sensors were assimilated only on domain 2. No observations were assimilated on the outer domain. In its current configuration, operational HWRF forecasts start from a cloud-free analysis, meaning that it will take some time to spin up a realistic cloud field during the forecast.

To reduce computational and storage expense, 126-h forecasts were only generated for forecasts starting at 0000 and 1200 UTC; however, full cycling still occurred at 6-h intervals, with shorter 12-h forecasts sufficient to start the next forecast cycle generated at 0600 and 1800 UTC. Sixteen 126-h forecasts initialized at 0000 or 1200 UTC were generated for each model configuration. In addition to the cumulus and microphysics schemes listed in Table 1, all simulations used the Noah land

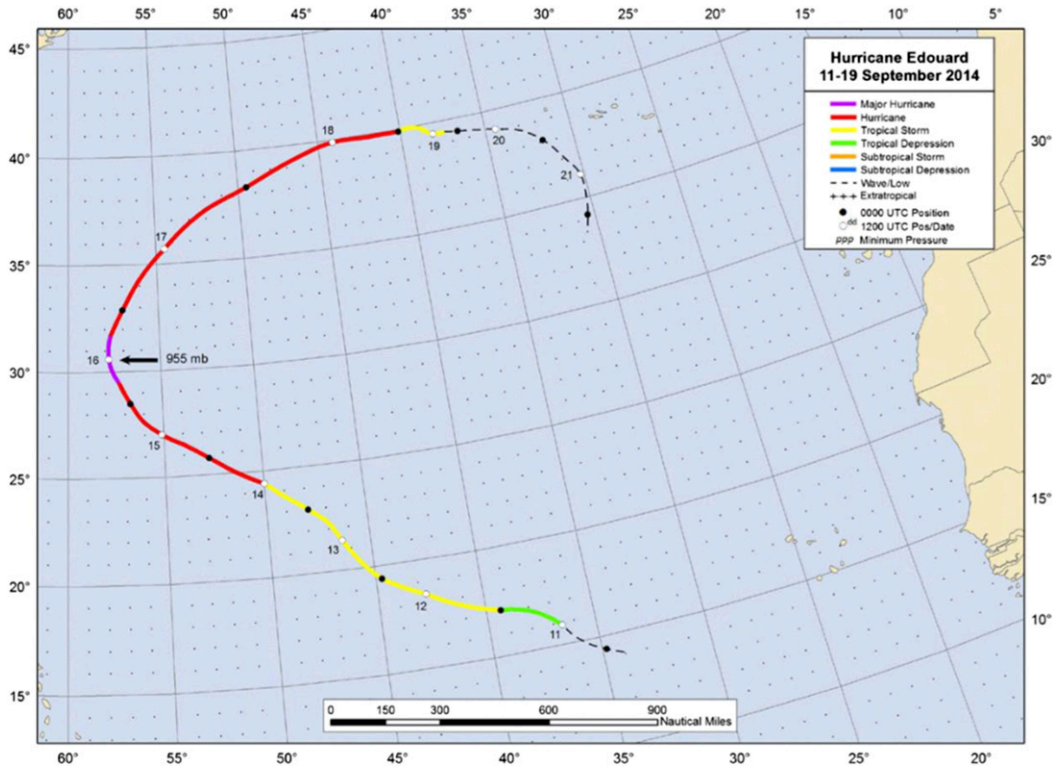

FIG. 1. National Hurricane Center best track position and intensity estimates shown at 12-h intervals from 11 to 19 Sep 2014. [Image obtained from Stewart (2014).]

surface model (Mitchell 2005), the GFS planetary boundary layer scheme (Hong and Pan 1996), and the Rapid Radiative Transfer Model for General Circulation Models longwave and shortwave radiation schemes with partial cloudiness (Iacono et al. 2008).

b. *Synthetic satellite brightness temperatures and forward model description*

The ability of each model configuration to accurately predict the cloud and water vapor fields is assessed through detailed comparisons of real and synthetic *Geostationary Operational Environmental Satellite-13* (*GOES-13*) infrared brightness temperatures. The Community Radiative Transfer Model (CRTM; Han et al. 2006) included in the Unified Post Processer (UPP) code was used to convert the model output into simulated infrared brightness temperatures. Model fields used by the CRTM include vertical profiles of temperature, water vapor mixing ratio, and the mixing ratios for each cloud hydrometeor species predicted by a given microphysics scheme, along with surface skin temperature and 10-m wind speed. Vertical profiles of effective particle diameters are also computed for each cloud hydrometeor species based on the assumptions made by each microphysics scheme (Otkin et al. 2007). With this method, the particle diameter varies as a function of mixing ratio and number concentration (when available), as occurs in real clouds. When only the mixing ratio is available for a given species, the number concentration is diagnosed using scheme-specific parameters, such as the slope intercept, and the assumed particle size distribution shape (e.g., Marshall–Palmer, etc.) for that species. A function was added to the community version of the UPP that correctly computes the effective diameters for the schemes evaluated during this study. Cloud absorption and scattering properties, such as extinction, single-scatter albedo, and full scattering phase function, are then assigned for each species using lookup tables that are a function of cloud mass and effective diameter. Infrared cloud optical depths are computed by scaling the visible optical depth by the ratio of the extinction efficiencies, whereas gas optical depths are computed using CompactOPTRAN code in the CRTM.

Simulated *GOES-13* brightness temperatures were computed at 6-h intervals during each forecast cycle, and subsequently remapped to the *GOES-13* projection to allow for direct comparisons of the real and simulated satellite data. The spectral bands used during this study include the 6.5-μm band that is sensitive to clouds and water vapor in the mid- and upper troposphere and the 10.7-μm window band that is sensitive to clouds when they are present or to surface skin temperature when skies are clear. Additional information about the accuracy of the forecast cloud field was obtained by passing the simulated infrared brightness temperatures through version 8.2.1 of the advanced Dvorak technique (ADT), which is a fully automated, objective method that is used to estimate TC intensity based on cloud patterns in geostationary satellite infrared imagery (Olander and Velden 2007). The ADT uses an objective scheme to identify the TC center location and to compute various cloud top parameters, such as the brightness temperature gradient between the eye and the surrounding central dense overcast region, that are indicators of TC intensity. It makes use of long-term statistical relationships to develop regression equations that are used to estimate the TC intensity. It can be used during all phases of the TC life cycle. Simulated ADT intensity estimates were computed at 6 h intervals during each forecast cycle using simulated GOES 10.7-μm imagery. The same version of the ADT algorithm was used to compute observed TC intensity estimates based on the observed GOES 10.7-μm imagery. A recent study by Manion et al. (2015) demonstrated that simulated ADT intensity estimates could provide an effective means to compare the accuracy of different parameterization schemes.

3. Results

a. *Upper-level cloud and water vapor analysis: Domain maps*

This section uses GOES 6.5-μm brightness temperatures to assess the accuracy of the forecast cloud and water vapor fields in the middle and upper troposphere. Figure 2 shows a representative comparison of the observed and simulated brightness temperatures from a 120-h forecast valid at 0000 UTC 18 September. The simulated images represent a combination of brightness temperatures on the two inner domains generated during the HWRF postprocessing step. Edouard had weakened into a category 1 hurricane by this time as it moved toward the northeast and encountered a less favorable environment. The hurricane was characterized by a small but well-defined eye enclosed within a decaying concentric eyewall (Abarca et al. 2016) (Fig. 2a). These features were depicted very differently in the forecasts, with most model configurations producing much larger eyes embedded within a large central dense overcast region. This behavior is consistent with several prior studies (e.g., Davis et al. 2008; Fierro et al. 2009; H. Jin et al. 2014) that have shown that unrealistically large hurricane eyes and circulation patterns can develop when the horizontal resolution is coarse. However, given that the inner domain contains 2-km grid spacing, the large eyes likely result from sensitivities to the model diffusion, surface physics, or other parameterization schemes (e.g., Rotunno et al.

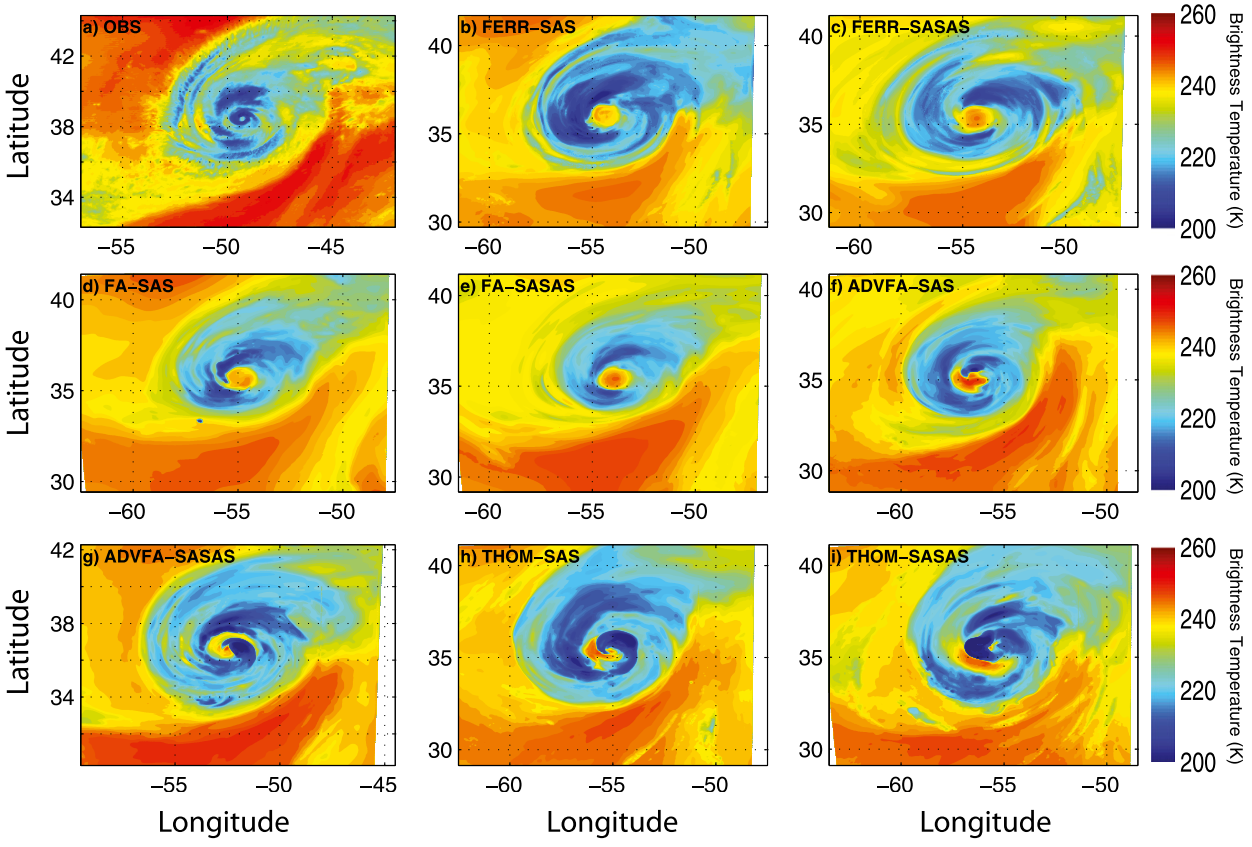

FIG. 2. Observed and simulated GOES 6.5-μm brightness temperatures valid at 0000 UTC 18 Sep 2014. The simulated images are from the 120-h forecast of the forecast cycle initialized at 0000 UTC 13 Sep 2014.

2009; Marks et al. 2016) rather than the spatial resolution. It is also possible that the eyes are too large due to the lack of an eyewall replacement cycle in the model forecasts.

Overall, it also apparent that all of the forecasts contain brightness temperatures that are colder than observed in the clear-sky areas to the northwest and south of the hurricane. This cold bias is illustrated by the lack of simulated brightness temperatures greater than 245 K. Because the 6.5-μm band is sensitive to water vapor, the cold bias indicates that the forecasts are too moist in the middle and upper troposphere, which is causing the peak of the satellite weighting function to occur at a higher, colder level of the atmosphere. Comparison of the cumulus scheme results shows that they also had a large impact on the water vapor content in the clear sky areas. For example, for each cloud microphysics scheme, the simulated brightness temperatures were 1–2 K warmer to the south of the hurricane when the SASAS cumulus scheme was used on the outer domains. The warmer brightness temperatures along the southern edge of the domain suggest that the SASAS cumulus scheme may have produced stronger subsidence on the outer domains that helped remove some of the moist bias in the upper troposphere prior to being advected into the inner domain through the lateral boundary conditions.

b. *Upper-level cloud and water vapor analysis: Probability distributions*

To examine the temporal evolution of errors in the upper level cloud and water vapor fields during the 126-h forecast period, 6.5-μm brightness temperature probability distributions were computed for each model configuration as a function of forecast hour using data from the eight forecast cycles that were initialized at 0000 UTC. The 1200 UTC forecasts were not included in this analysis to avoid cancelling errors that are a function of the diurnal cycle. Probability distributions were also computed for the corresponding observations at each forecast verification time, with differences subsequently computed between the observed and simulated distributions. The resultant differences for the inner domain are shown in Fig. 3. Blue colors indicate that the model forecasts do not contain enough grid points with brightness temperatures of a certain value, whereas red colors indicate that they contain too many.

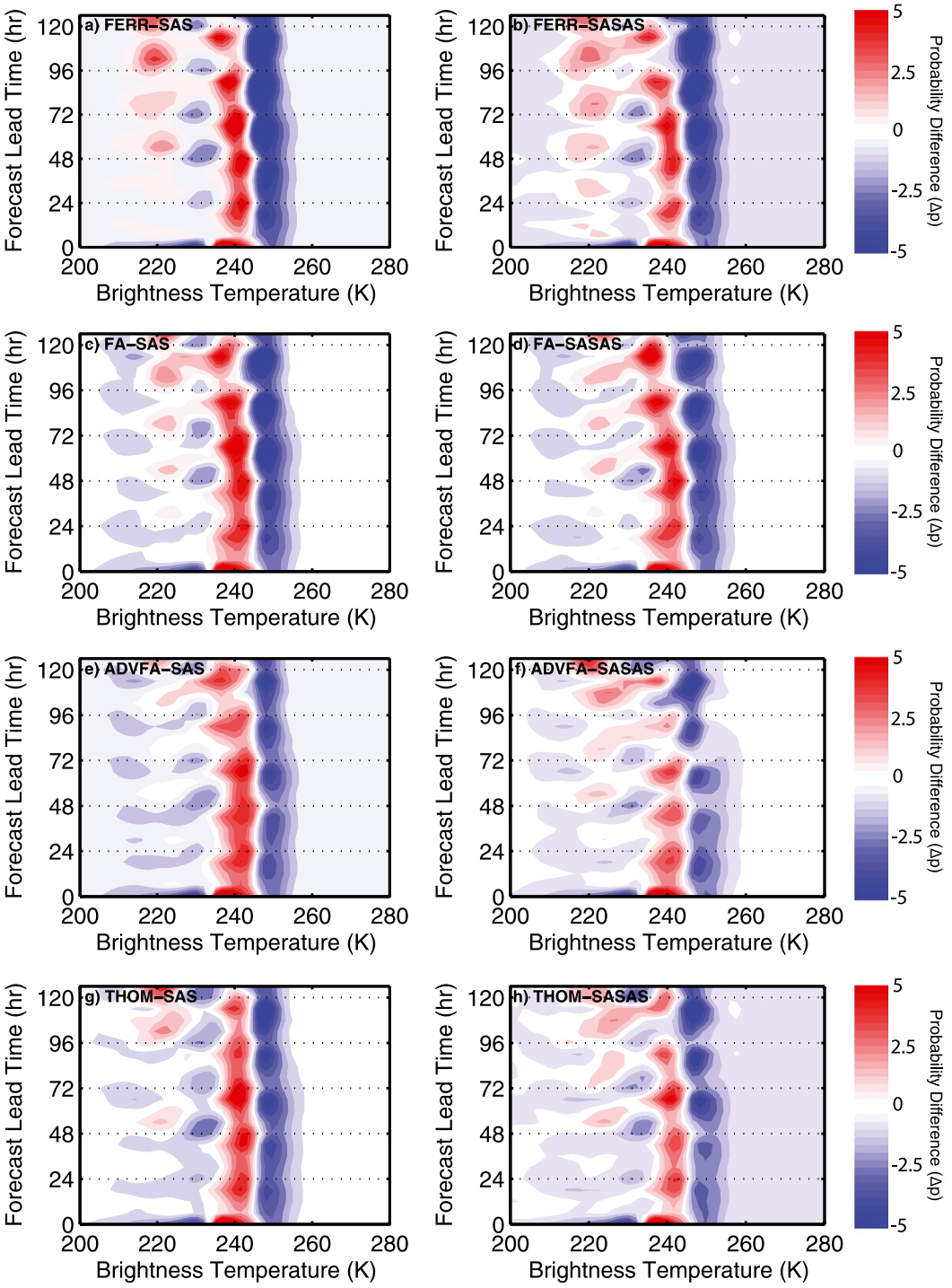

FIG. 3. Forecast-minus-observed GOES 6.5-μm brightness temperature probability distribution differences plotted as a function of forecast hour for each model configuration. The probability distributions were computed using data from all forecasts initialized at 0000 UTC.

Overall, the most notable feature on each panel is the red–blue couplet that occurs during the entire forecast period. This couplet shows that all of the model configurations produce too many (few) grid points with cold (warm) brightness temperatures, which is consistent with what was shown in Fig. 2. The overabundance of cold brightness temperatures will by necessity lead to a deficiency of warmer brightness temperatures given the

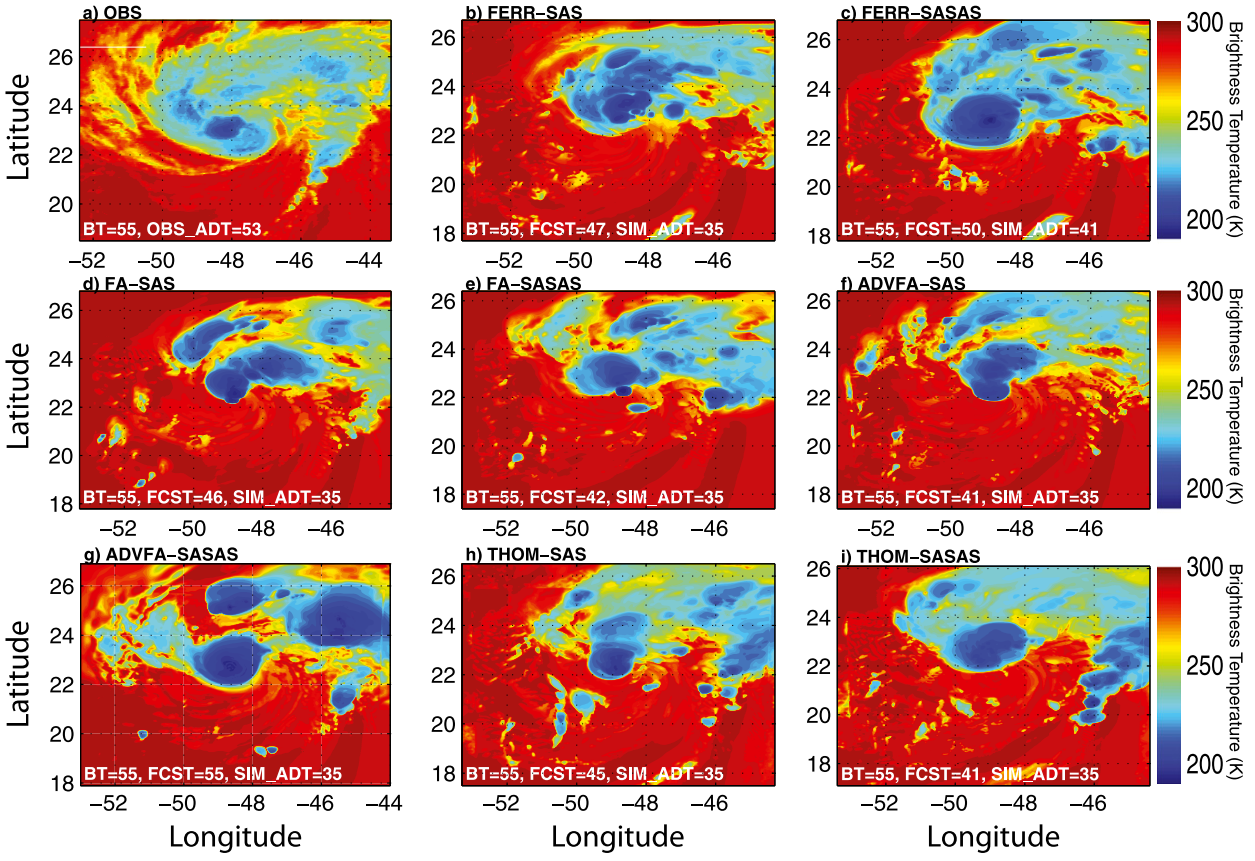

FIG. 4. Observed and simulated GOES 10.7-μm brightness temperatures valid at 0000 UTC 14 Sep 2014. Cyclone intensity metrics from the best track (BT) dataset, forecast maximum sustained 10-m wind speeds (FCST), and satellite-derived ADT (SIM_ADT) are shown on each panel. The simulated imagery and intensity metrics are from the 24-h forecast of the forecast cycle initialized at 0000 UTC 13 Sep 2014.

top-down nature of this satellite-based analysis. As discussed in the previous section, this shift toward colder brightness temperatures indicates that there is too much water vapor in the middle and upper troposphere. Because this moist bias is present at the beginning of the forecast period, this indicates that it is at least partially due to a moist bias in the GFS analyses used to initialize the HWRF forecasts, which is consistent with a recent study by Ren (2016) that documented similarly large biases in the GFS model. Comparison of the microphysics schemes also reveals large differences during the forecast, with the FERR and FA schemes exhibiting the largest bias overall whereas the initial bias remains the same or decreases with time when the other schemes are used. For each microphysics scheme, simulations using the SASAS cumulus scheme typically contained smaller errors for brightness temperatures between 235 and 255 K. This is especially evident for the ADVFA and THOM simulations during the last few days of the forecast. Together, these results show that the parameterization schemes and how they interact with other model physics is leading to different responses to the same initial water vapor bias in the upper troposphere. In addition, given that the cumulus schemes were not used on the inner domain, the strong sensitivity of these errors to the cumulus scheme also illustrates the importance of assessing the model accuracy on the outer domains and the behavior of the parameterization schemes at coarser resolutions. Further work is necessary to explore these sensitivities in greater detail.

Another interesting feature in Fig. 3 is the large diurnal cycle that occurs for each model configuration during the entire forecast period for brightness temperatures less than 235 K. This error pattern is primarily driven by differences in the diurnal cycle of deep convection and its subsequent impact on the cloud and moisture fields in the upper troposphere. Most of the model configurations produce too many clouds with brightness temperatures around 220 K and not enough near 230 K, especially during later forecast hours. They also tend to slightly underpredict the frequency of the coldest clouds with brightness temperatures <215 K. This complex error pattern suggests a general tendency for most of the configurations to produce clouds that are optically thicker or higher than observed within the

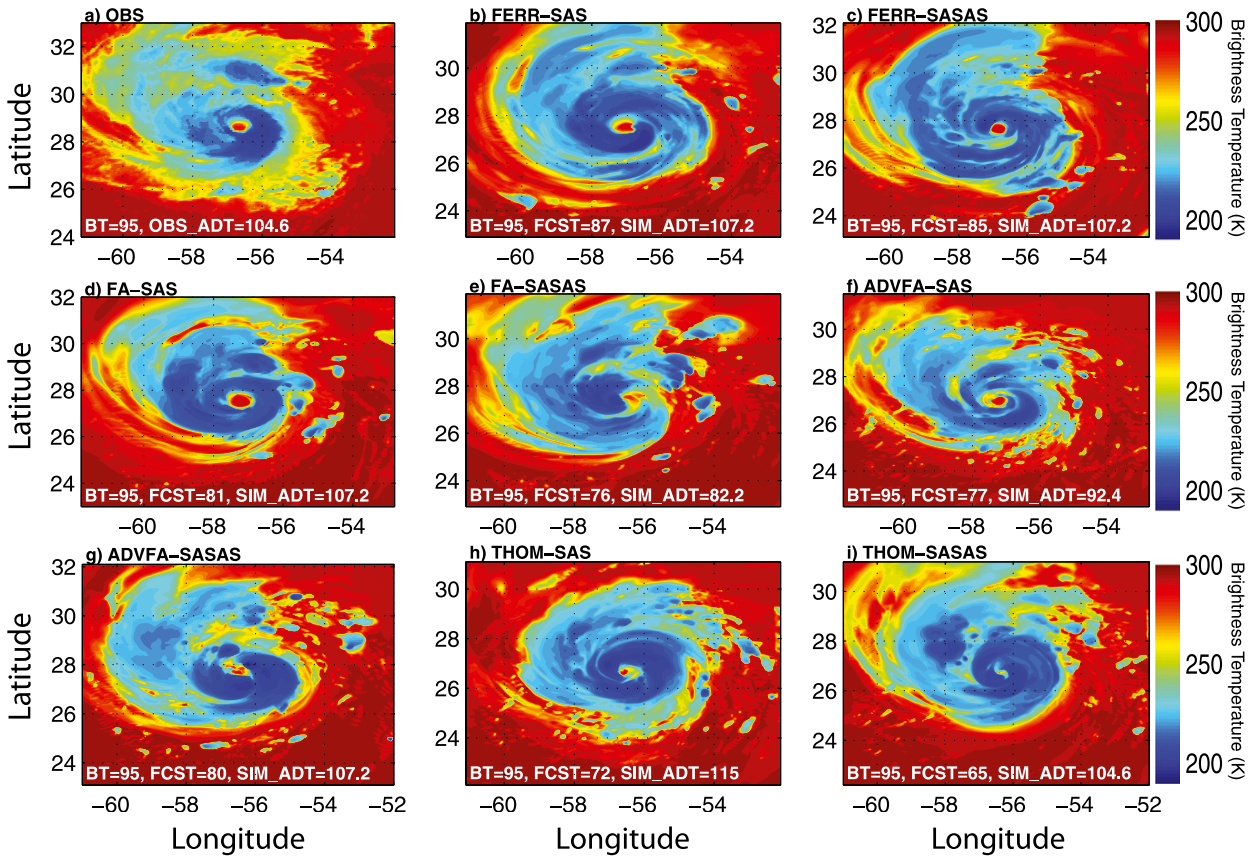

FIG. 5. As in Fig. 4, but corresponding to the 72-h forecast valid at 0000 UTC 16 Sep 2014.

upper-level cloud shield associated with the TC (e.g., refer to Fig. 2), while simultaneously underpredicting the spatial extent of the deepest convective clouds containing the coldest brightness temperatures. This tendency toward colder brightness temperatures, however, could also be caused by a bias in the CRTM used to compute the simulated brightness temperatures. This topic will be briefly explored in Section 3g.

c. *Intensity assessment using the advanced Dvorak technique*

In this section, the overall accuracy of the forecast cloud field on the inner domain is assessed through comparison of TC intensity estimates from the ADT algorithm with maximum sustained 10-m wind speeds from the NHC hurricane BT dataset and HWRF Model forecasts (FCST) for a representative forecast cycle. The FCST intensities were obtained using the Geophysical Fluid Dynamics Laboratory vortex tracker algorithm used by the operational HWRF Model to estimate the vortex center position and provide TC intensity and structure metrics. Figure 4 shows the observed and simulated 10.7-μm brightness temperatures and intensity estimates from a 24-h forecast valid at 0000 UTC 14 September. At this time, the BT and ADT intensity metrics both indicated that Edouard was a strong tropical storm (Fig. 4a). The observed satellite imagery depicts a strengthening system characterized by a well-defined circulation with an area of deep convection near the storm center (Fig. 4a). Inspection of the model results shows that all of the forecasts have surface winds that are weaker than observed, with the simulated ADT intensities being even weaker. The weak bias in the ADT estimates does not represent a problem with the ADT algorithm; instead, it indicates that 24 h is not enough time for the HWRF Model to spin up a completely realistic cloud field after starting from a cloud-free analysis. The weaker ADT intensity estimates are consistent with the more disorganized appearance of the simulated cloud field and the weaker surface circulations found in the model forecasts.

By the 72-h forecast valid at 0000 UTC 16 September (Fig. 5), Edouard had developed into a strong category 2 hurricane with maximum sustained winds of 95 kt according to the BT dataset. The satellite imagery reveals a very strong cyclone characterized by a well-defined

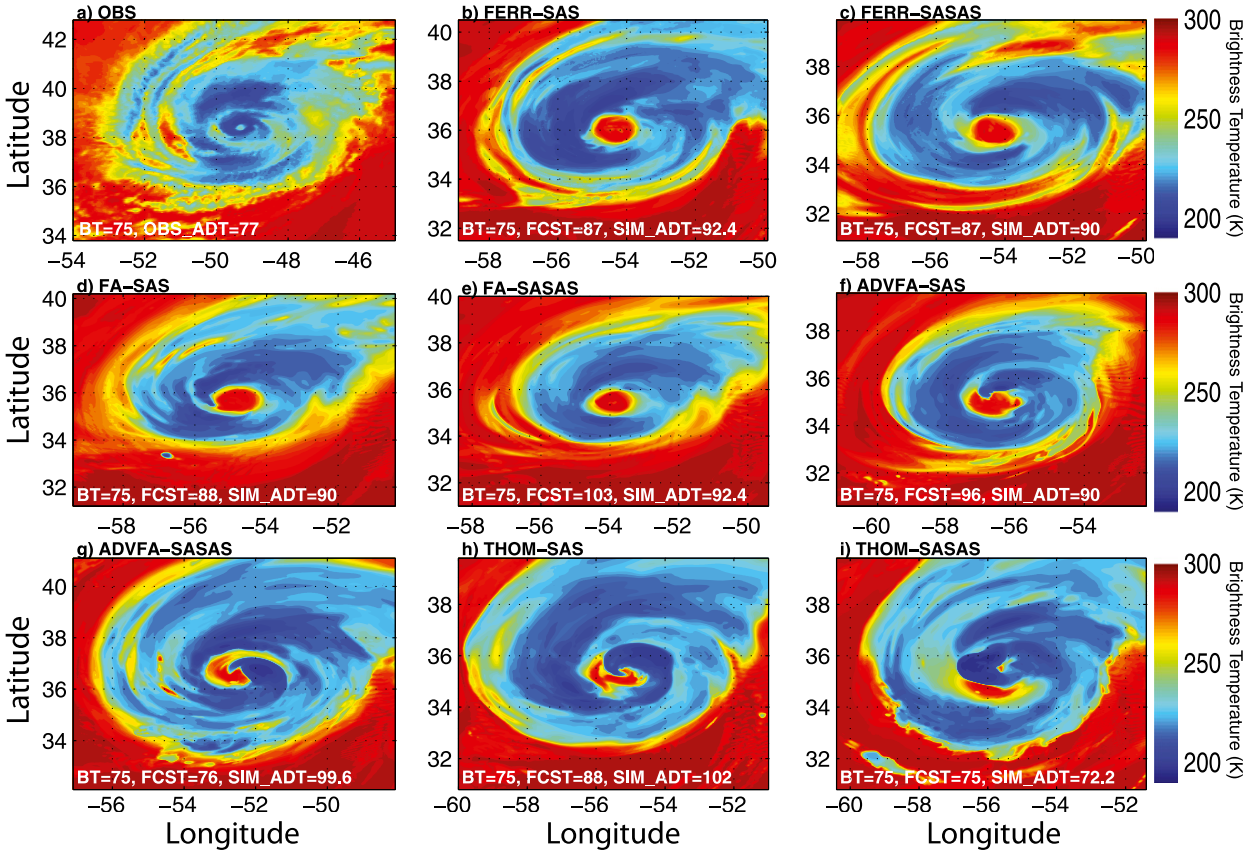

FIG. 6. As in Fig. 4, but corresponding to the 120-h forecast valid at 0000 UTC 18 Sep 2014.

eye surrounded by a large central dense overcast region (Fig. 5a). All of the surface-based intensities from the model forecasts were weaker than observed, with the FERR (THOM) forecasts having the strongest (weakest) surface winds. The simulated ADT intensity estimates were stronger than the FCST wind speeds for all of the model configurations and exhibited a wide range of values that are consistent with differences in the forecast cloud field. For example, the cloud field in the FA–SASAS simulation (Fig. 5e) has a somewhat ragged appearance consistent with the relatively weak 82-kt ADT intensity estimate. Likewise, the THOM-SAS forecast has a small eye surrounded by a nearly circular central dense overcast region containing very cold brightness temperatures that is consistent with the much stronger 115-kt ADT intensity estimate (Fig. 5h). Many of the forecasts exhibit a large spread between the FCST and ADT intensity metrics that indicates that there can be a large disconnect between TC intensity based on forecast 10-m wind speeds and that inferred by cloud patterns in the simulated satellite imagery. Differences between these two metrics are especially large when the THOM scheme is used. In most cases, however, the simulated ADT intensities are actually a closer match to the observed BT intensity than were the FCST 10-m wind speeds.

By 0000 UTC 18 September, Edouard was in the latter stages of an eyewall replacement cycle that had caused it to weaken into a category 1 hurricane according to the BT and ADT intensity datasets (Fig. 6a). Comparison to the 120-h forecasts shows that very large differences had developed between the observed and simulated cloud fields for the different parameterization schemes. For example, the upper level cloud field is much smaller during the FA forecasts than it is during the FERR and THOM forecasts. The spatial extent of the coldest brightness temperatures in these upper-level cloud features is much larger than observed, which is consistent with the probability differences shown in Fig. 3. Also, unlike earlier in the forecast, the surface and ADT intensities are generally stronger than observed. The most notable feature in most of the images however is the very large hurricane eye that stands in sharp contrast to the small eye and double eyewall structure found in the observations. Though the more intense hurricanes and large eyes are at least partially due to the lack of an eyewall replacement cycle in the model forecasts, the eyes are still much larger than is typically observed.

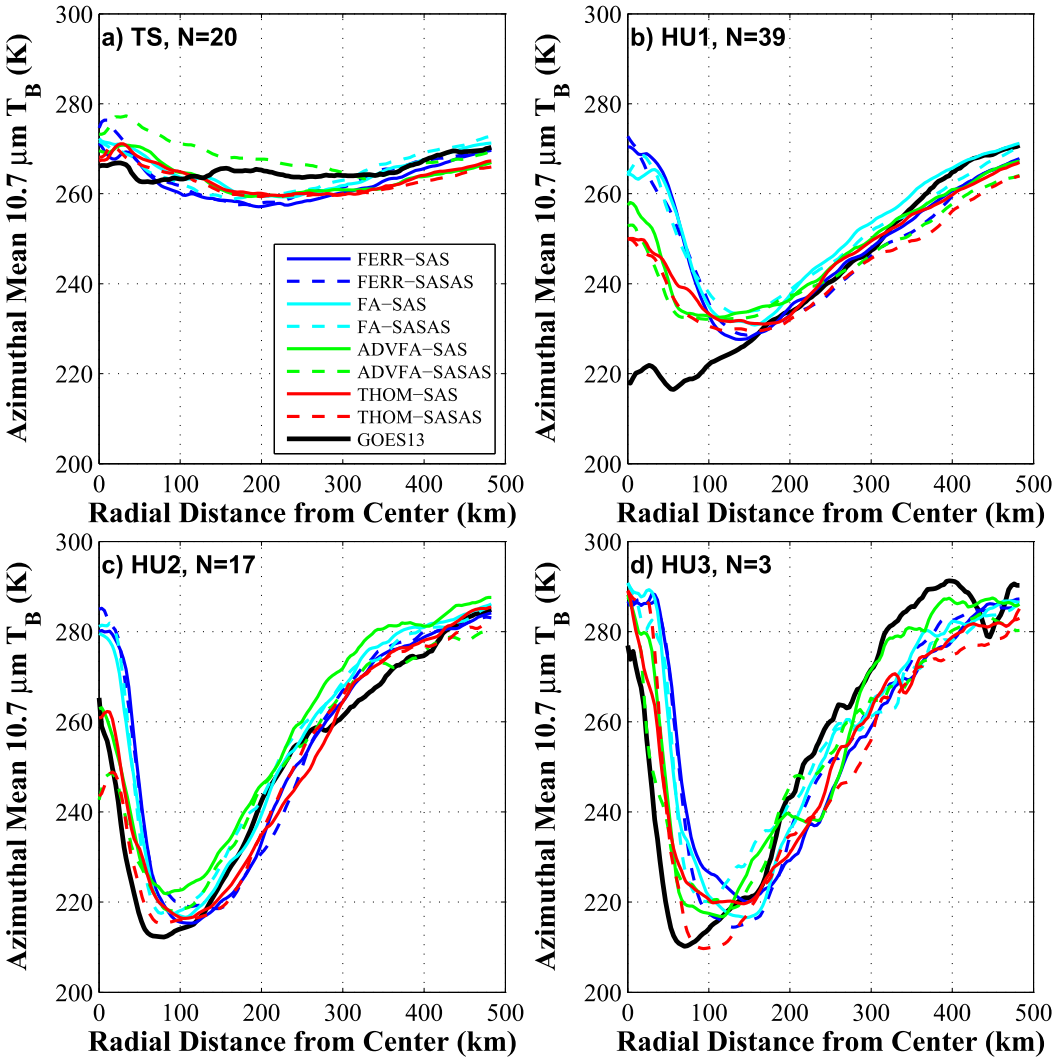

FIG. 7. Azimuthal mean 10.7-μm brightness temperature distributions extending from the tropical cyclone center to a distance of 500 km for the observations and each model configuration separated into (a) tropical storm and (b)–(d) category 1–3 hurricanes. The sample size N is shown on each panel.

d. Azimuthal cloud structure

In this section, we will use the observed and simulated GOES 10.7-μm brightness temperatures to examine the azimuthal structure of the forecast cloud field for different TC intensities. Figure 7 shows the azimuthal mean brightness temperatures extending from the TC center to a distance of 500 km for each model configuration and for the observations. The observed cyclone center was obtained from the hurricane BT dataset whereas the grid point with the lowest mean sea level pressure was used to determine the center of the forecast TC. The observed TC intensity obtained at 6-h intervals was used to aggregate the results into each TC intensity category before computing the observed and simulated azimuthal mean brightness temperatures. Model output from each forecast cycle initialized at 1200 UTC was used to construct these distributions; however, data prior to the 30-h forecast for each forecast cycle was not included in order to limit the impact of the spin-up process on the cloud field.

Overall, all of the model configurations realistically captured the nearly constant brightness temperature distributions for tropical storm strength disturbances (Fig. 7a). For category 1 hurricanes, however, all of them contain brightness temperatures that are much warmer than observed for radial distances less than 75 km before becoming similar beyond 150 km (Fig. 7b). The warmer brightness temperatures near the storm center indicate that the hurricane eye is clearer in the forecasts than it

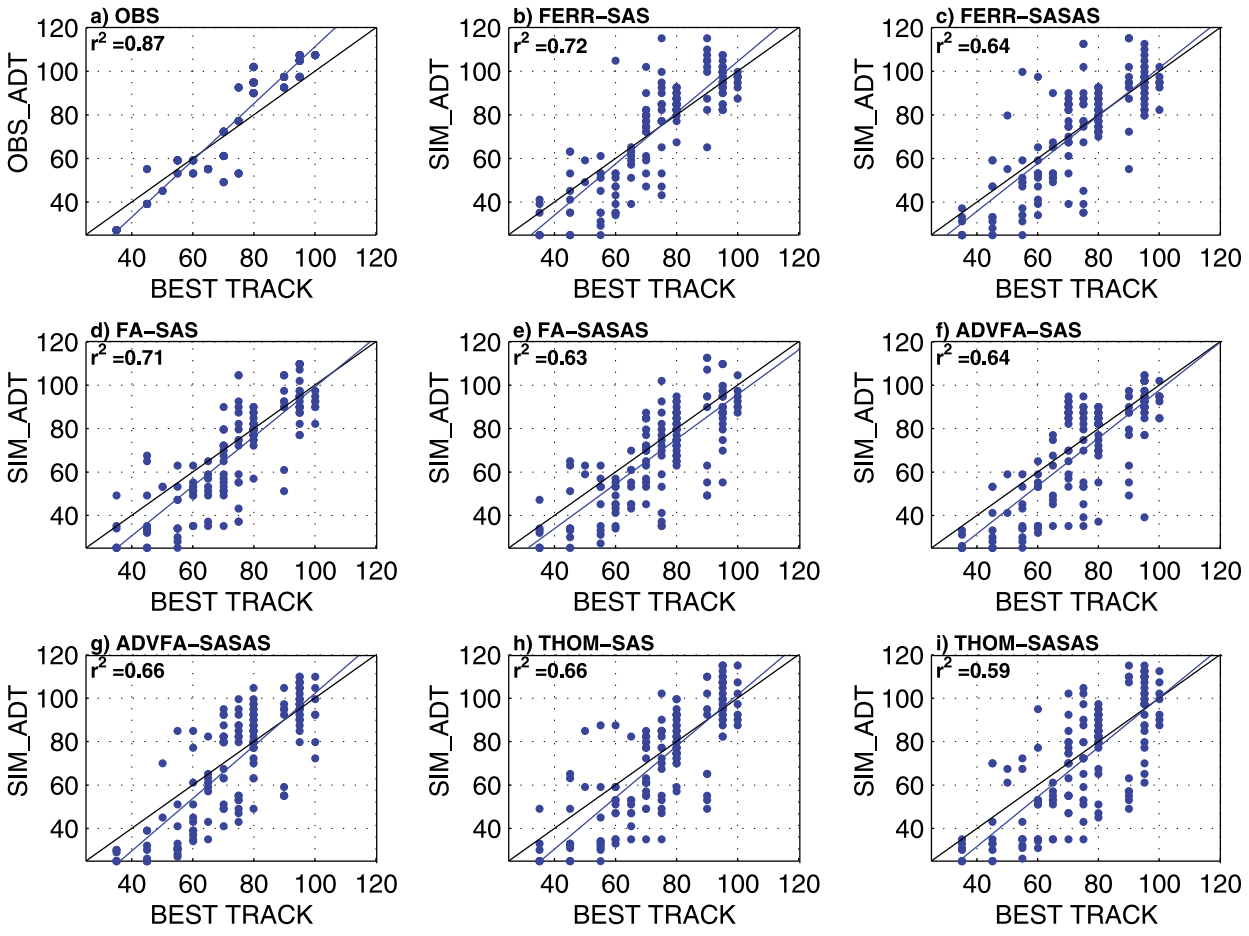

FIG. 8. Scatterplots of satellite-derived ADT and hurricane best track intensity estimates for the observations and each model configuration accumulated at 6-h intervals over a 6-day period from 0000 UTC 13 Sep to 0000 UTC 19 Sep 2014.

was in the observations. This warm bias is partially due to the tendency for some HWRF forecasts to produce very large eyes during the decay phase of Hurricane Edouard, such as that shown in Fig. 6. The observed brightness temperatures had warmed substantially for radial distances <50 km by the time Eduoard had become a category 2 hurricane (Fig. 7c). The brightness temperature distributions closely matched the observations when the THOM and ADVFA microphysics schemes were used; however, they continued to be too warm near the TC center when the FERR and FA schemes were used. For category 3 hurricanes (Fig. 7d), the simulated brightness temperatures continued to be too warm near the TC center, with the warmer temperatures extending to a greater radial distance than observed. These results further reveal that the FERR and FA schemes are most susceptible to producing unrealistically large eyes for all hurricane intensities, whereas the smaller eye diameters found in the THOM and ADVFA forecasts are more accurate.

e. Relationship between ADT and 10-m wind speed intensities

To more thoroughly assess the accuracy of the forecast cloud field using the ADT, Fig. 8 shows scatterplots of observed and model-derived ADT intensity estimates versus the BT intensity accumulated at 6-h intervals over a 6-day period from 0000 UTC 13 September to 0000 UTC 19 September. Because the HWRF forecasts start from a cloud-free analysis, simulated ADT intensities prior to the 30-h forecast are excluded from the scatterplots to limit the impact of the model spinup process on the cloud field. Overall, there is a strong relationship between the observed ADT and BT intensities as evidenced by a correlation of 0.87 (Fig. 8a). There is a tendency however for the ADT estimates to be slightly weaker (stronger) than the BT intensities when Edouard was a weak (strong) TC. Though the correlations are weaker, a similar relationship was found for each of the model configurations, with the

highest correlations obtained for forecasts using the FERR and FA microphysics schemes or the SAS cumulus scheme. The tendency for the simulated ADT intensities to be weaker than observed when Edouard was a tropical storm suggests that the spatial pattern of the cloud field was less organized or that there was less deep convection in the forecasts similar to what was shown in Fig. 4.

The consistency between the forecast TC intensities obtained directly from the model-predicted lower-tropospheric wind speeds with those inferred from cloud patterns in the simulated satellite infrared imagery is assessed using Fig. 9. These scatterplots were constructed using model output from the same observation and forecast time periods used in Fig. 8. Overall, the correlations indicate broad agreement between the surface 10-m wind speeds and the TC intensity implied by the structure of the cloud field. The ADT intensities tend to be weaker than the FCST 10-m wind speeds when the maximum sustained wind speeds are less than 60 kt. Absolute differences between the ADT and FCST intensity metrics become larger for more intense TCs; however, they still remain similar on a percentage basis when scaled by the observed intensity. The simulated ADT intensities exhibit little or no bias for the FERR and FA schemes when the FCST 10-m wind speeds are greater than 60 kt. This stands in contrast to the propensity for the THOM and ADVFA forecasts to have ADT intensity estimates that are much stronger than the surface-based intensities. For the hurricane intensities examined during this study, the presence of an eye along with its size are typically the most important parameters that influence the ADT intensity estimates. As was shown in section 3d, both of these schemes tend to produce hurricanes with smaller eyes than the FERR and FA schemes. Though the smaller eyes more closely match the observations, they are typically indicative of more intense hurricanes, and will generally lead to higher ADT intensity estimates.

Colder brightness temperatures in the central dense overcast region can also lead to higher ADT-derived intensities; therefore, the presence of a cold bias during some of the forecasts (e.g., Fig. 5) could also be contributing to the positive ADT intensity bias for some of the stronger storms. Inspection of the azimuthal brightness temperature averages (Fig. 7); however, shows that with the exception of the brightness temperatures within the first 100 km of the TC center (which are warmer than observed), the simulated brightness temperatures are similar to the observations when averaged over all forecasts. Together, these characteristics suggest that the primary cause of the positive ADT intensity bias for observed BT intensities >70 kt is that the HWRF forecasts tend to have eye features that are clearer and more prominent than observed. In addition, it is important to note that the positive bias in the simulated ADT intensity estimates for the stronger hurricanes during the ADVFA and THOM forecasts is mostly with respect to the FCST 10-m wind speeds (e.g., Fig. 9), whereas the bias is not as large when the simulated ADT intensity estimates are compared to the observed BT dataset (Fig. 8). This behavior suggests that at least some of the apparent bias may actually be due to the HWRF Model producing a weaker surface cyclone than observed rather than the ADT intensities being too strong.

f. Forecast error time series

This section assesses the evolution of the track and intensity errors during the 5-day forecast period with respect to the BT dataset. Figure 10 shows a comparison of traditional error metrics computed using the mean sea level pressure and 10-m wind speed forecasts to intensity errors computed using the ADT intensity estimates. Overall, the track errors are similar for all model configurations through forecast hour 60 and then diverge at later forecast hours (Fig. 10a). Among the microphysics schemes, the largest errors occur during the THOM forecasts, whereas forecasts using the FERR and FA schemes contain the smallest errors. A similar stratification occurs for the maximum sustained 10-m wind speeds (Fig. 10b) with the exception that the ADVFA forecasts tend to have the largest errors on average. Sensitivity in the track and intensity forecasts to the cumulus parameterization scheme varies with time and among the various microphysics schemes, thereby making it difficult to determine which cumulus scheme produced the most accurate forecasts during this case study. Though all of the model configurations begin the forecast period with essentially no wind speed bias (Fig. 10d), a negative bias develops thereafter and reaches its maximum magnitude between forecast hours 36 and 48 before diminishing during later forecast hours. The ADVFA and THOM schemes are most susceptible to producing storms that are weaker than observed. The FERR scheme had the smallest wind speed bias and produced the most accurate forecasts based on these traditional verification metrics.

Inspection of the ADT intensity errors shows that all of the model configurations contain very large errors at the beginning of the forecast period due to the lack of clouds in the initialization datasets (Figs. 10c,e). The large weak bias and mean absolute errors rapidly decrease during the first 24 h of the forecast as the model spins up a more realistic cloud field. Based on the wind speed bias (Fig. 10e), the FERR scheme is able to

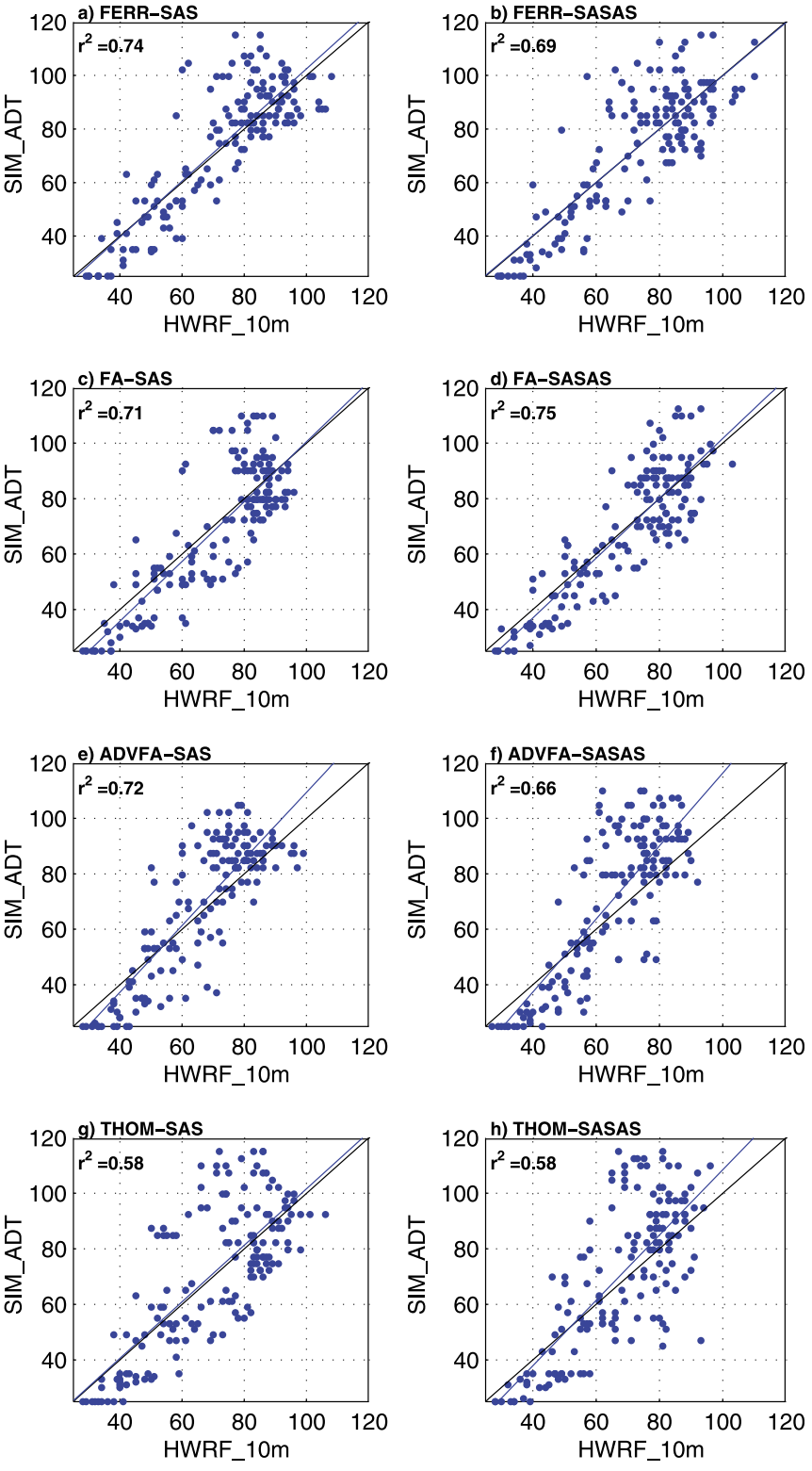

FIG. 9. Scatterplots of satellite-derived ADT intensity estimates and forecast maximum sustained 10-m wind speeds for each model configuration accumulated at 6-h intervals over a 6-day period from 0000 UTC 13 Sep to 0000 UTC 19 Sep.

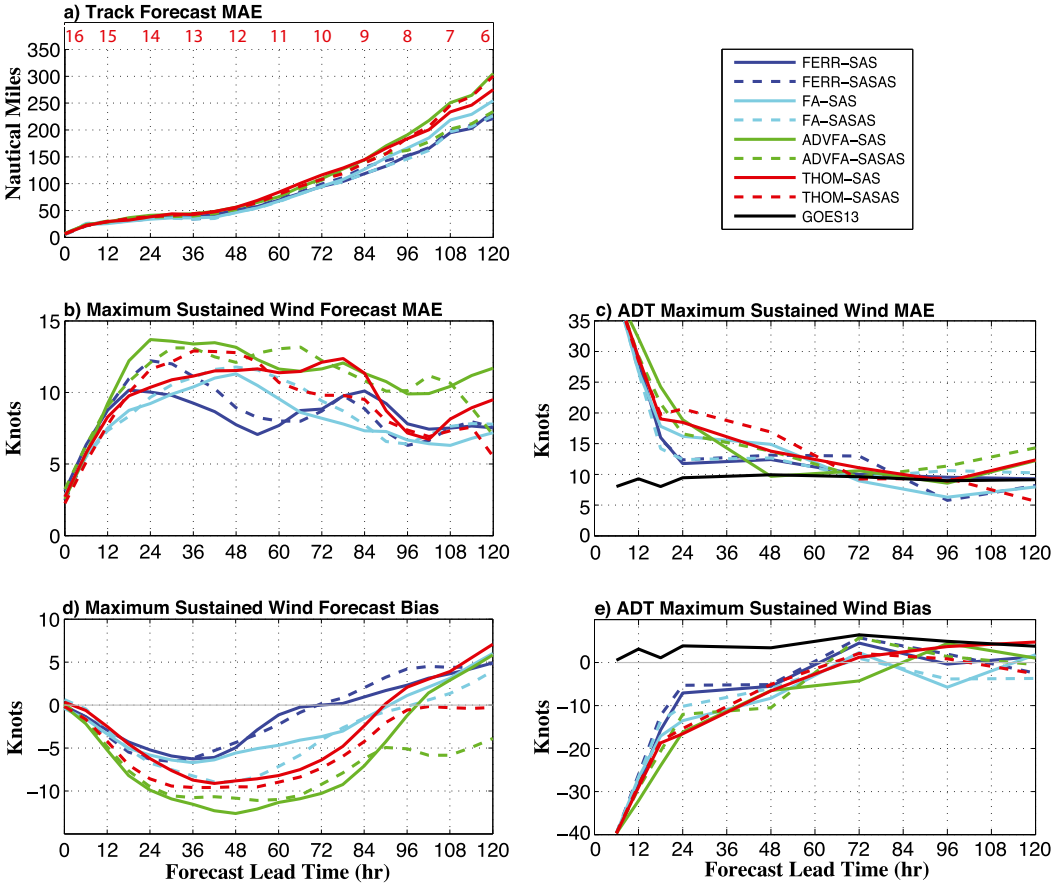

FIG. 10. HWRF tropical cyclone (a) track errors computed using the forecast minimum sea level pressure and (b) intensity and (d) intensity bias errors computed using the forecast maximum 10-m wind speed. The corresponding ADT-estimated (c) intensity and (e) intensity bias errors are also shown. All errors are computed with respect to the hurricane best track position and wind speed datasets and averaged over all forecast cycles. Errors are plotted as a function of forecast hour. The sample size for each forecast hour is shown along the top of (a).

produce a realistic cloud field more quickly than the other schemes and thus has the smallest ADT intensity bias between forecast hours 18 and 48. Even so, a negative bias persists up to the 60 h forecast in the ADT intensities and up to the 90 h forecast in the 10-m wind speeds for most model configurations. Though not examined during this study, large differences in the spatial and temporal distribution of latent heating could at least partially account for the tendency for weaker TCs during the first few days of the forecasts. This is possible given that the model must spin up a complete cloud field at the beginning of each forecast rather than starting with a cloud field that accurately captures the latent heating distribution in the central dense overcast region and spiral rainbands. This possibility is supported by the tendency for the wind forecast errors (Figs. 10b,d) to steadily increase during the first 24 h until the ADT intensity estimates derived from patterns in the cloud field finally stabilize (Figs. 10c,e). The forecast wind speed errors then slowly decrease with time after a more realistic cloud field has developed. Together, these results indicate that most of the model spin-up process is complete within the first 24–36 h of the forecast, but that some detrimental impacts of the spin-up process continue to affect the forecasts beyond this time.

g. *Case study comparing different forward radiative transfer models*

Comparison of the observed and simulated brightness temperatures in sections 3c and 3d revealed that the simulated brightness temperatures tend to be too cold in regions containing upper-level clouds. Here, we briefly explore the sensitivity of these errors to the forward radiative transfer model. Though beyond the scope of the current study to explore this topic in detail, limited sensitivity tests were performed using the successive order of interaction (SOI; Heidinger et al. 2006) forward radiative transfer model to see if its use could reduce the magnitude of the cold bias in the upper-level clouds. The

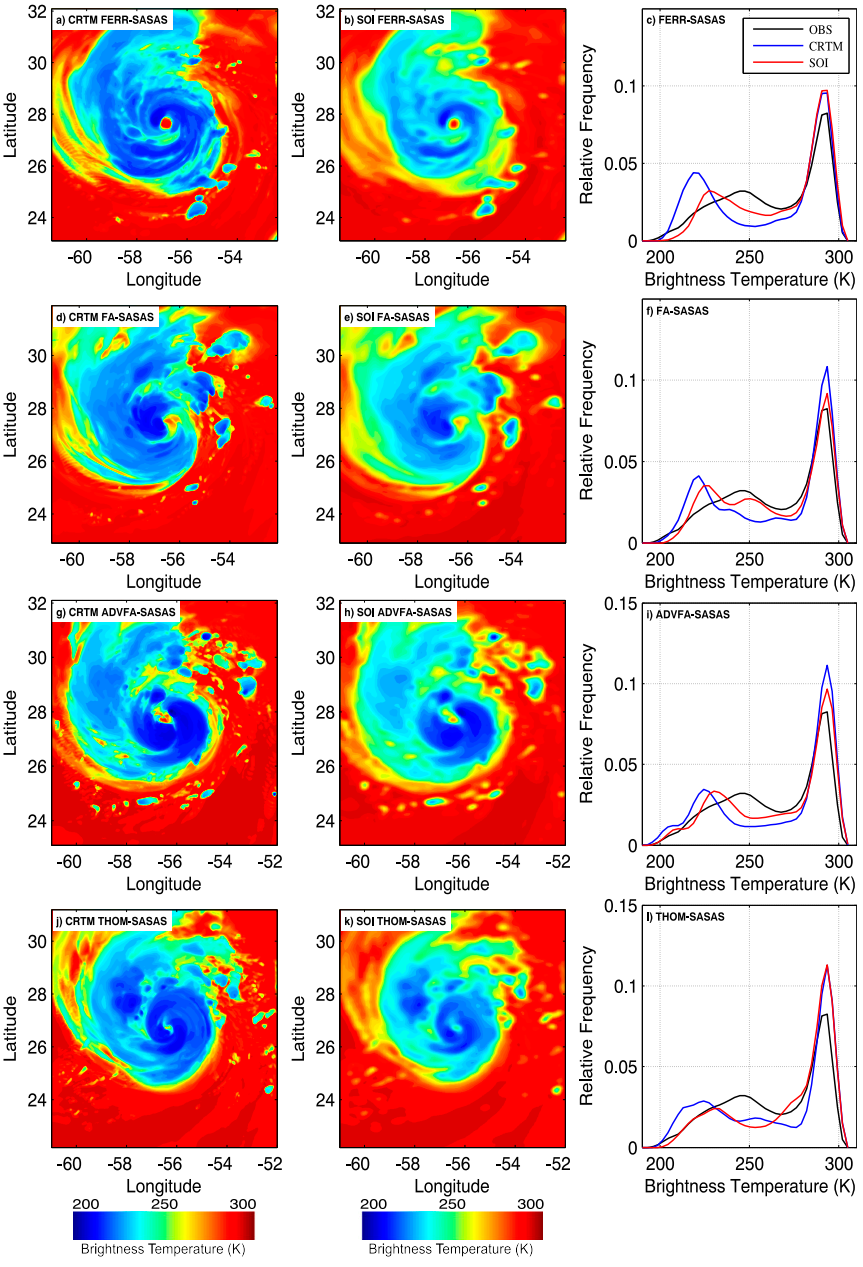

FIG. 11. Simulated GOES 10.7-μm brightness temperatures computed using the CRTM and SOI forward radiative transfer models along with the corresponding observed and simulated 10.7-μm brightness temperature probability distributions from a 72-h forecast valid at 0000 UTC 16 Sep 2014. Results are shown for the (a)–(c) FERR-SASAS, (d)–(f) FA-SASAS, (g)–(i) ADVFA-SASAS, and (j)–(l) THOM-SASAS forecasts.

SOI model has been used in prior model validation and data assimilation studies (Cintineo et al. 2014; Otkin 2010, 2012; Jones et al. 2013) and has proven to be capable of producing accurate brightness temperatures in both clear and cloudy-sky conditions. A key difference in the SOI compared to the CRTM is its use of the Baum et al. (2005) cloud property lookup tables that are used to determine the ice cloud scattering and absorption properties, such as single scatter albedo, extinction efficiency, and the full scattering phase function.

Figure 11 shows a comparison of the simulated 10.7-μm brightness temperatures computed using the CRTM and SOI models for a 72-h forecast valid at 0000 UTC 16 September 2014. The corresponding observed and simulated

brightness temperature probability distributions are also shown. For brevity, this figure only includes results from forecasts in which the microphysics schemes were paired to the SASAS cumulus scheme. Overall, it is evident that the simulated brightness temperatures in cloudy regions tend to be much warmer when the SOI model is used. Inspection of the probability distributions shows that this warming generally resulted in a more accurate depiction, especially for mid and upper-level clouds characterized by brightness temperatures <275 K. This improvement is illustrated by the shift in the peak of the distributions near 220 K toward warmer values and the increase in brightness temperatures between 275 and 240 K. This example reveals that it may be possible to remove some of this cold bias through use of different cloud property lookup tables in the forward radiative transfer models used to compute simulated brightness temperatures. Preliminary tests indicate that the Baum et al. (2005) ice scattering phase functions used by the SOI permit more forward scattering of radiation, thereby leading to warmer brightness temperatures when ice clouds are present. A more thorough analysis exploring this topic in greater detail will be presented in a future study.

4. Discussion and conclusions

In this study, cycled forecast experiments were performed to assess the ability of different cloud microphysics and cumulus parameterization schemes in the HWRF Model to accurately simulate the cloud and water vapor fields. Data assimilation and other model updates were performed at 6-h intervals during the entire life cycle of Hurricane Edouard, with full 126-h forecasts initiated each day at 0000 and 1200 UTC. The forecast accuracy was assessed through comparison of observed and simulated *GOES-13* infrared brightness temperatures and through a detailed assessment of satellite-derived ADT TC intensity estimates. The CRTM was used to convert the model-predicted water vapor, cloud, and temperature fields into simulated infrared brightness temperatures that were then passed through the ADT algorithm to produce TC intensity estimates. Four cloud microphysics and two cumulus parameterization schemes were assessed.

Evaluation of the 6.5-μm brightness temperatures revealed the presence of a large moist bias in the middle and upper troposphere during the entire forecast period and for all model configurations. Because the moist bias was present at the beginning of the forecasts, this indicates that the excessive water vapor content was at least partially due to a moist bias in the GFS analyses used to initialize the HWRF Model forecasts. There was some sensitivity to the parameterization schemes, with the FERR microphysics scheme having the largest bias and the THOM and ADVFA schemes having the smallest bias. This suggests that having separate advection terms for each cloud hydrometeor species limited the size of the bias. The bias was further reduced when the SASAS cumulus scheme was used. There was also a large diurnal cycle in the brightness temperature errors that was related to errors in the diurnal cycle of deep convection and its impact on the cloud and water vapor fields in the upper troposphere. It is important to note that the operational HWRF Model in its current configuration does not assimilate any satellite observations on the outer domain. Thus, assimilation of satellite infrared brightness temperatures sensitive to water vapor could potentially reduce the moist bias in the initialization datasets. This in turn should lead to more accurate forecasts; however, it may also necessitate retuning the parameterization schemes given their different responses to the moist bias.

Comparison of observed and simulated 10.7-μm brightness temperature imagery and mean azimuthal brightness temperature distributions showed that all of the model configurations produced hurricane eyes that were larger and clearer than observed, especially for later forecast hours. The tendency to produce unrealistically large eyes was most noticeable for the FERR and FA microphysics schemes and occurred for all hurricane intensities. The THOM and ADVFA schemes produced the most accurate brightness temperature distributions and eye diameters, though the eyes were still larger than observed. These results using satellite infrared brightness temperatures are consistent with prior studies that used more traditional wind radii metrics to document unrealistically large hurricane eyes in model simulations. As discussed in section 3a, prior studies have shown that unrealistically large eyes can result from coarse model resolution or biases in the surface physics and planetary boundary layer schemes. The results from this study indicate that the eye size is also sensitive to the microphysics scheme. Additional work is necessary to explore this sensitivity in greater detail.

The accuracy of the forecast cloud field was also assessed using satellite-derived ADT TC intensity estimates. Comparisons to the forecast 10-m wind speeds showed that there is reasonable agreement between the surface-based intensities and the ADT TC intensities inferred via cloud patterns in the upper troposphere. The FERR and FA schemes had the strongest correlations between these intensity metrics with no intensity bias evident for the stronger storms. Forecasts using the ADVFA and THOM schemes, however, exhibited much larger differences for hurricane-strength storms, with the ADT intensity estimates typically being stronger than the

10-m wind speeds. This result reveals that there is often a large disconnect between the forecast TC intensity based on maximum sustained winds near the surface and that implied by forecast cloud patterns in the upper troposphere when these microphysics schemes are used. The ADT intensity metrics provided a powerful means to document and evaluate these differences. More research is necessary to determine the cause of this discrepancy because it may be one of the reasons why the ADVFA and THOM schemes produce more accurate hurricane eye diameters, yet also have larger track and intensity errors than the FERR and FA schemes. Given the longer history of the FERR and FA schemes in the HWRF Model, it is possible that their superior track and intensity forecasts in spite of having less accurate cloud fields could be due to better tuning with the other model parameterization schemes.

Finally, the largest forecast differences were typically found when comparing the microphysics schemes. This forecast sensitivity has also been shown in previous studies and illustrates the importance of the cloud microphysics scheme for TC prediction. An interesting result was that the ADVFA scheme behaved more like the THOM scheme than the FA scheme from which it is derived. Preliminary tests have shown that this behavior appears to be primarily driven by enhanced vertical transport of graupel into the upper troposphere in areas with deep convection that then impacts the evolution of the cloud field. Ongoing work is exploring this sensitivity in greater detail. The cumulus scheme had a large impact on the upper-level water vapor bias, with forecasts using the newer SASAS scheme containing a smaller bias than the SAS scheme, but otherwise the impact was minimal or negative. This is consistent with recent work by Biswas et al. (2014) that showed that new cumulus schemes have yet to demonstrate superior forecast skill in the operational HWRF Model when compared to the original SAS scheme. More extensive analyses using satellite infrared and microwave brightness temperatures are necessary to refine these results.

Acknowledgments. This study was supported by the NOAA Hurricane Forecast Improvement Project under Grant NA14NWS4680026. All HWRF Model simulations and analysis tasks were performed on the "jet" supercomputer located at the NOAA/Earth System Research Laboratory. Very valuable and detailed comments from three anonymous reviewers helped improve the manuscript. We also thank Vijay Tallapragada, Ligia Bernardet, Frank Marks, and Kate Musgrave for valuable discussions and Kate Fossell and Sarah Griffin for assistance implementing the forward radiative transfer models.

REFERENCES

Abarca, S. F., M. T. Montgomery, S. A. Braun, and J. Dunion, 2016: On the secondary eyewall formation of Hurricane Edouard (2014). *Mon. Wea. Rev.*, **144**, 3321–3331, doi:10.1175/MWR-D-15-0421.1.

Aligo, E., B. Ferrier, J. Carley, E. Rodgers, M. Pyle, S. J. Weiss, and I. L. Jirak, 2014: Modified microphysics for use in high resolution NAM forecasts. *27th Conf. on Severe Local Storms*, Madison, WI, Amer. Meteor. Soc., 16A.1. [Available online at https://ams.confex.com/ams/27SLS/webprogram/Paper255732.html.]

Arakawa, A., and W. H. Schubert, 1974: Interaction of a cumulus cloud ensemble with the large-scale environment, Part I. *J. Atmos. Sci.*, **31**, 674–701, doi:10.1175/1520-0469(1974)031<0674:IOACCE>2.0.CO;2.

——, and C.-M. Wu, 2013: A unified representation of deep moist convection in numerical modeling of the atmosphere. Part I. *J. Atmos. Sci.*, **70**, 1977–1992, doi:10.1175/JAS-D-12-0330.1.

Bao, J.-W., S. G. Gopalakrishnan, S. A. Michelson, F. D. Marks, and M. T. Montgomery, 2012: Impact of physics representations in the HWRFX on simulated hurricane structure and pressure–wind relationships. *Mon. Wea. Rev.*, **140**, 3278–3299, doi:10.1175/MWR-D-11-00332.1.

Baum, B. A., P. Yang, A. J. Heymsfield, S. Platnick, M. D. King, Y.-X. Hu, and S. T. Bedka, 2005: Bulk scattering properties for the remote sensing of ice clouds. Part II: Narrowband models. *J. Appl. Meteor.*, **44**, 1896–1911, doi:10.1175/JAM2309.1.

Bernardet, L., and Coauthors, 2015: Community support and transition of research to operations for the Hurricane Weather Research and Forecasting Model. *Bull. Amer. Meteor. Soc.*, **96**, 953–960, doi:10.1175/BAMS-D-13-00093.1.

Bikos, D., and Coauthors, 2012: Synthetic satellite imagery for real-time high-resolution model evaluation. *Wea. Forecasting*, **27**, 784–795, doi:10.1175/WAF-D-11-00130.1.

Biswas, M. K., L. Bernardet, and J. Dudhia, 2014: Sensitivity of hurricane forecasts to cumulus parameterizations in the HWRF model. *Geophys. Res. Lett.*, **41**, 9113–9119, doi:10.1002/2014GL062071.

Chaboureau, J.-P., and J.-P. Pinty, 2006: Validation of a cirrus parameterization with Meteosat Second Generation observations. *Geophys. Res. Lett.*, **33**, L03815, doi:10.1029/2005GL024725.

——, J.-P. Cammas, P. Mascart, J.-P. Pinty, C. Claud, R. Roca, and J.-J. Morcrette, 2000: Evaluation of a cloud system life-cycle simulated by the Meso-NH model during FASTEX using METEOSAT radiances and TOVS-3I cloud retrievals. *Quart. J. Roy. Meteor. Soc.*, **126**, 1735–1750, doi:10.1002/qj.49712656609.

Cintineo, R., J. A. Otkin, F. Kong, and M. Xue, 2014: Evaluating the accuracy of planetary boundary layer and cloud microphysical parameterization schemes in a convection-permitting ensemble using synthetic *GOES-13* satellite observations. *Mon. Wea. Rev.*, **142**, 163–182, doi:10.1175/MWR-D-13-00143.1.

Davis, C. A., and L. F. Bosart, 2002: Numerical simulations of the genesis of Hurricane Diana. Part II: Sensitivity of track and intensity prediction. *Mon. Wea. Rev.*, **130**, 1100–1124, doi:10.1175/1520-0493(2002)130<1100:NSOTGO>2.0.CO;2.

——, and Coauthors, 2008: Prediction of landfalling hurricanes with the Advanced Hurricane WRF Model. *Mon. Wea. Rev.*, **136**, 1990–2005, doi:10.1175/2007MWR2085.1.

Deshpande, M. S., S. Pattnaik, and P. S. Salvekar, 2012: Impact of cloud parameterization on the numerical simulation of a

super cyclone. *Ann. Geophys.*, **30**, 775–795, doi:10.5194/angeo-30-775-2012.

Elsberry, R., T. D. B. Lambert, and M. A. Boothe, 2007: Accuracy of Atlantic and eastern North Pacific tropical cyclone intensity forecast guidance. *Wea. Forecasting*, **22**, 747–762, doi:10.1175/WAF1015.1.

Feltz, W. F., K. M. Bedka, J. A. Otkin, T. Greenwald, and S. A. Ackerman, 2009: Understanding satellite-observed mountain wave signatures using high-resolution numerical model data. *Wea. Forecasting*, **24**, 76–86, doi:10.1175/2008WAF2222127.1.

Ferrier, B. S., 2005: An efficient mixed-phase cloud and precipitation scheme for use in operational NWP models. *Eos, Trans. Amer. Geophys. Union*, **86** (Spring Meeting Suppl.), Abstract A42A-02.

Fierro, A. O., R. F. Rogers, and F. D. Marks, 2009: The impact of horizontal grid spacing on the microphysical and kinematic structures of strong tropical cyclones simulated with the WRF-ARW Model. *Mon. Wea. Rev.*, **137**, 3717–3743, doi:10.1175/2009MWR2946.1.

Fovell, R. G., and H. Su, 2007: Impact of cloud microphysics on hurricane track forecasts. *Geophys. Res. Lett.*, **34**, L24810, doi:10.1029/2007GL031723.

——, and K. L. Corbosiero, 2009: Cloud microphysics impact on hurricane track as revealed in idealized experiments. *J. Atmos. Sci.*, **66**, 1764–1778, doi:10.1175/2008JAS2874.1.

——, ——, A. Seifert, and K.-N. Liou, 2010: Impact of cloud-radiative processes on hurricane track. *Geophys. Res. Lett.*, **37**, L07808, doi:10.1029/2010GL042691.

Gopalakrishnan, S. G., S. Goldenberg, T. Quirino, X. Zhang, F. Marks Jr., K. Yeh, R. Atlas, and V. Tallapragada, 2012: Towards improving high-resolution numerical hurricane forecasting: Influence of model horizontal grid resolution, initialization, and physics. *Wea. Forecasting*, **27**, 647–666, doi:10.1175/WAF-D-11-00055.1.

Grasso, L. D., and T. Greenwald, 2004: Analysis of 10.7-μm brightness temperatures of a simulated thunderstorm with two-moment microphysics. *Mon. Wea. Rev.*, **132**, 815–825, doi:10.1175/1520-0493(2004)132<0815:AOMBTO>2.0.CO;2.

——, M. Sengupta, J. F. Dostalek, R. Brummer, and M. DeMaria, 2008: Synthetic satellite imagery for current and future environmental satellites. *Int. J. Remote Sens.*, **29**, 4373–4384, doi:10.1080/01431160801891820.

——, D. T. Lindsey, K.-S. Sunny Lim, A. J. Clark, D. Bikos, and S. R. Dembek, 2014: Evaluation of and suggested improvements to the WSM6 microphysics in WRF-ARW using synthetic and observed *GOES-13* imagery. *Mon. Wea. Rev.*, **142**, 3635–3650, doi:10.1175/MWR-D-14-00005.1.

Grell, G. A., 1993: Prognostic evaluation of assumptions used by cumulus parameterizations. *Mon. Wea. Rev.*, **121**, 764–787, doi:10.1175/1520-0493(1993)121<0764:PEOAUB>2.0.CO;2.

Han, Y., P. Van Delst, Q. Liu, F. Weng, B. Yan, R. Treadon, and J. Derber, 2006: JCSDA Community Radiative Transfer Model (CRTM)—Version 1. NOAA Tech. Rep. NESDIS 122, 40 pp. [Available online at https://docs.lib.noaa.gov/noaa_documents/NESDIS/TR_NESDIS/TR_NESDIS_122.pdf.]

Heidinger, A. K., C. O'Dell, R. Bennartz, and T. Greenwald, 2006: The successive-order-of-interaction radiative transfer model. Part I: Model development. *J. Appl. Meteor. Climatol.*, **45**, 1388–1402, doi:10.1175/JAM2387.1.

Hong, S.-Y., and H.-L. Pan, 1996: Nonlocal boundary layer vertical diffusion in a medium-range forecast model. *Mon. Wea. Rev.*, **124**, 2322–2339, doi:10.1175/1520-0493(1996)124<2322:NBLVDI>2.0.CO;2.

Houze, R. A., Jr., S. S. Chen, B. F. Smull, W.-C. Lee, and M. M. Bell, 2007: Hurricane intensity and eyewall replacement. *Science*, **315**, 1235–1239, doi:10.1126/science.1135650.

Iacono, M. J., J. S. Delamere, E. J. Mlawer, M. W. Shephard, S. A. Clough, and W. D. Collins, 2008: Radiative forcing by long-lived greenhouse gases: Calculations with the AER radiative transfer models. *J. Geophys. Res.*, **113**, D13103, doi:10.1029/2008JD009944.

Jankov, I., and Coauthors, 2011: An evaluation of five ARW-WRF microphysics schemes using synthetic GOES imagery for an atmospheric river event affecting the California coast. *J. Hydrometeor.*, **12**, 618–633, doi:10.1175/2010JHM1282.1.

Jin, H., M. S. Peng, Y. Jin, and J. D. Doyle, 2014: An evaluation of the impact of horizontal resolution on tropical cyclone predictions using COAMPS-TC. *Wea. Forecasting*, **29**, 252–270, doi:10.1175/WAF-D-13-00054.1.

Jin, Y., and Coauthors, 2014: The impact of ice phase cloud parameterizations on tropical cyclone prediction. *Mon. Wea. Rev.*, **142**, 606–625, doi:10.1175/MWR-D-13-00058.1.

Jones, T. A., J. A. Otkin, D. J. Stensrud, and K. Knopfmeier, 2013: Assimilation of satellite infrared radiances and Doppler radar observations during a cool season observing system simulation experiment. *Mon. Wea. Rev.*, **141**, 3273–3299, doi:10.1175/MWR-D-12-00267.1.

Kaplan, J., M. DeMaria, and J. A. Knaff, 2010: A revised tropical cyclone rapid intensification index for the Atlantic and eastern North Pacific basins. *Wea. Forecasting*, **25**, 220–241, doi:10.1175/2009WAF2222280.1.

Karlsson, K.-G., 1996: Validation of modeled cloudiness using satellite-estimated cloud climatologies. *Tellus*, **48A**, 767–785, doi:10.1034/j.1600-0870.1996.t01-1-00015.x.

Lee, C.-Y., M. K. Tippett, A. H. Sobel, and S. J. Carmago, 2016: Rapid intensification and the bimodal distribution of tropical cyclone intensity. *Nat. Commun.*, **7**, 10625, doi:10.1038/ncomms10625.

Liu, C., and M. W. Moncrieff, 2007: Sensitivity of cloud resolving simulations of warm-season convection to cloud microphysics parameterizations. *Mon. Wea. Rev.*, **135**, 2854–2868, doi:10.1175/MWR3437.1.

Lopez, P., K. Finkele, P. Clark, and P. Mascart, 2003: Validation and intercomparison of three FASTEX cloud systems: Comparison with coarse-resolution simulations. *Quart. J. Roy. Meteor. Soc.*, **129**, 1841–1871, doi:10.1256/qj.01.113.

Manion, A., C. Evans, T. Olander, C. S. Velden, and L. D. Grasso, 2015: An evaluation of advanced Dvorak technique–derived tropical cyclone intensity estimates during extratropical transition using synthetic satellite imagery. *Wea. Forecasting*, **30**, 984–1009, doi:10.1175/WAF-D-15-0019.1.

Marks, F., K. J. Sellwood, and S. Abarca, 2016: Evaluation of the HWRF radius of maximum wind using Doppler radar analyses. *32nd Conf. on Hurricanes and Tropical Meteorology*, San Juan, PR, Amer. Meteor. Soc., 10.1. [Available online at https://ams.confex.com/ams/32Hurr/webprogram/Paper293852.html.]

Mitchell, K., 2005: The community Noah land surface model (LSM). NOAA/NCEP/Environmental Modeling Center, 26 pp. [Available online at http://www.ral.ucar.edu/research/land/technology/lsm/noah/Noah_LSM_USERGUIDE_2.7.1.pdf.]

Mukhopadhyay, P., S. Taraphdar, and B. N. Goswami, 2011: Influence of moist processes on track and intensity forecast of cyclones over the north Indian Ocean. *J. Geophys. Res.*, **116**, D05116, doi:10.1029/2010JD014700.

Nasrollahi, N., A. AghaKouchak, J. Li, X. Gao, K. Hsu, and S. Sorooshian, 2012: Assessing the impacts of different WRF

precipitation physics in hurricane simulations. *Wea. Forecasting*, **27**, 1003–1016, doi:10.1175/WAF-D-10-05000.1.

Olander, T. L., and C. S. Velden, 2007: The advanced Dvorak technique: Continued development of an objective scheme to estimate tropical cyclone intensity using geostationary infrared satellite imagery. *Wea. Forecasting*, **22**, 287–298, doi:10.1175/WAF975.1.

Otkin, J. A., 2010: Clear and cloudy sky infrared brightness temperature assimilation using an ensemble Kalman filter. *J. Geophys. Res.*, **115**, D19207, doi:10.1029/2009JD013759.

——, 2012: Assimilation of water vapor sensitive infrared brightness temperature observations during a high impact weather event. *J. Geophys. Res.*, **117**, D19203, doi:10.1029/2012JD017568.

——, and T. J. Greenwald, 2008: Comparison of WRF model-simulated and MODIS-derived cloud data. *Mon. Wea. Rev.*, **136**, 1957–1970, doi:10.1175/2007MWR2293.1.

——, D. J. Posselt, E. R. Olson, H.-L. Huang, J. E. Davies, J. Li, and C. S. Velden, 2007: Mesoscale numerical weather prediction models used in support of infrared hyperspectral measurement simulation and product algorithm development. *J. Atmos. Oceanic Technol.*, **24**, 585–601, doi:10.1175/JTECH1994.1.

——, T. J. Greenwald, J. Sieglaff, and H.-L. Huang, 2009: Validation of a large-scale simulated brightness temperature dataset using SEVIRI satellite observations. *J. Appl. Meteor. Climatol.*, **48**, 1613–1626, doi:10.1175/2009JAMC2142.1.

Pattnaik, S., and T. N. Krishnamurti, 2007a: Impact of cloud microphysical processes on hurricane intensity. Part 1: Control run. *Meteor. Atmos. Phys.*, **97**, 117–126, doi:10.1007/s00703-006-0247-y.

——, and ——, 2007b: Impact of cloud microphysical processes on hurricane intensity. Part 2: Sensitivity experiments. *Meteor. Atmos. Phys.*, **97**, 127–147, doi:10.1007/s00703-006-0248-x.

——, C. Inglish, and T. N. Krishnamurti, 2011: Influence of rain-rate initialization, cloud microphysics, and cloud torques on hurricane intensity. *Mon. Wea. Rev.*, **139**, 627–649, doi:10.1175/2010MWR3382.1.

Ren, L., 2016: A case study of GOES-15 imager bias characterization with a numerical weather prediction model. *Front. Earth Sci.*, **10**, 409–418, doi:10.1007/s11707-016-0579-y.

Rikus, L., 1997: Application of a scheme for validating clouds in an operational global NWP model. *Mon. Wea. Rev.*, **125**, 1615–1637, doi:10.1175/1520-0493(1997)125<1615:AOASFV>2.0.CO;2.

Rotunno, R., Y. Chen, W. Wang, C. Davis, J. Dudhia, and G. J. Holland, 2009: Large-eddy simulation of an idealized tropical cyclone. *Bull. Amer. Meteor. Soc.*, **90**, 1783–1788, doi:10.1175/2009BAMS2884.1.

Smith, R. K., and G. L. Thomsen, 2010: Dependence of tropical cyclone intensification on the boundary layer representation in a numerical model. *Quart. J. Roy. Meteor. Soc.*, **136**, 1671–1685, doi:10.1002/qj.687.

Stewart, S. R., 2014: Tropical cyclone report: Hurricane Edouard (AL062014). National Hurricane Center, 19 pp. [Available online at http://www.nhc.noaa.gov/data/tcr/AL062014_Edouard.pdf.]

Sun, Z., and L. Rikus, 2004: Validating model clouds and their optical properties using geostationary satellite imagery. *Mon. Wea. Rev.*, **132**, 2006–2020, doi:10.1175/1520-0493(2004)132<2006:VMCATO>2.0.CO;2.

Tallapragada, V., and Coauthors, 2015: Hurricane Weather Research and Forecasting (HWRF) Model: 2015 scientific documentation. Developmental Testbed Center, 119 pp. [Available online at http://www.dtcenter.org/HurrWRF/users/docs/.]

Thompson, G., P. R. Field, R. M. Rasmussen, and W. D. Hall, 2008: Explicit forecasts of winter precipitation using an improved bulk microphysics scheme. Part II: Implementation of a new snow parameterization. *Mon. Wea. Rev.*, **136**, 5095–5115, doi:10.1175/2008MWR2387.1.

——, M. Tewari, K. Ikeda, S. Tessendorf, C. Weeks, J. A. Otkin, and F. Kong, 2016: Explicitly-coupled cloud physics and radiation parameterizations and subsequent evaluation in WRF high-resolution convective forecasts. *Atmos. Res.*, **168**, 92–104, doi:10.1016/j.atmosres.2015.09.005.

Tselioudis, G., and C. Jakob, 2002: Evaluation of midlatitude cloud properties in a weather and a climate model: Dependence on dynamic regime and spatial resolution. *J. Geophys. Res.*, **107**, 4781, doi:10.1029/2002JD002259.

Van Weverberg, K., and Coauthors, 2013: The role of cloud microphysics parameterization in the simulation of mesoscale convective system clouds and precipitation in the tropical western Pacific. *J. Atmos. Sci.*, **70**, 1104–1128, doi:10.1175/JAS-D-12-0104.1.

Wang, X., D. Parrish, D. Kleist, and J. Whitaker, 2013: GSI 3DVar-based ensemble–variational hybrid data assimilation for NCEP Global Forecast System: Single-resolution experiments. *Mon. Wea. Rev.*, **141**, 4098–4117, doi:10.1175/MWR-D-12-00141.1.

Wang, Y., 2009: How do outer spiral rainbands affect tropical cyclone structure and intensity? *J. Atmos. Sci.*, **66**, 1250–1273, doi:10.1175/2008JAS2737.1.

Wu, L., and B. Wang, 2001: Effects of convective heating on movement and vertical coupling of tropical cyclones: A numerical study. *J. Atmos. Sci.*, **58**, 3639–3649, doi:10.1175/1520-0469(2001)058<3639:EOCHOM>2.0.CO;2.

Yablonsky, R. M., I. Ginis, B. Thomas, V. Tallapragada, D. Sheinin, and L. Bernardet, 2015: Description and analysis of the ocean component of NOAA's operational Hurricane Weather Research and Forecasting Model (HWRF). *J. Atmos. Oceanic Technol.*, **32**, 144–163, doi:10.1175/JTECH-D-14-00063.1.

Zhu, P., and Coauthors, 2015: Impact of subgrid-scale processes on eyewall replacement cycle of tropical cyclones in HWRF system. *Geophys. Res. Lett.*, **42**, 10 027–10 036, doi:10.1002/2015GL066436.